www.ann-phys.org

adp

# annalen der physik

WILEY-VCH

Ann. Phys. (Berlin) 527, No. 9–10, 713–722 (2015) / DOI 10.1002/andp.201500110

annalen der physik



# Anderson transition for Google matrix eigenstates

*O. V. Zhirov*[1,2] *and D. L. Shepelyansky*[3,*]

Received 2 February 2015, revised 20 February 2015, accepted 20 February 2015
Published online 16 March 2015

We introduce a number of random matrix models describing the Google matrix $G$ of directed networks. The properties of their spectra and eigenstates are analyzed by numerical matrix diagonalization. We show that for certain models it is possible to have an algebraic decay of PageRank vector with the exponent similar to real directed networks. At the same time the spectrum has no spectral gap and a broad distribution of eigenvalues in the complex plain. The eigenstates of $G$ are characterized by the Anderson transition from localized to delocalized states and a mobility edge curve in the complex plane of eigenvalues.

## 1 Introduction

The phenomenon of Anderson localization [1] appears in a variety of quantum physical systems including electron transport in disordered solids and waves in random media (see e.g. [2, 3]). It is usually analyzed in the frame of Hermitian or unitary matrices. Recently, the localization properties of nonunitary complex matrices has been analyzed for Euclidean matrices [4] in relation to light and wave localization [5].

In this work we analyze the possibilities of Anderson like localization and delocalization for the matrices belonging to the class of Markov chains and Google matrix $G$ [6, 7]. Such matrices have real nonnegative elements with the sum of elements in each column being equal to unity. For a directed network one first defines an adjacency matrix $A_{ij}$ which has element 1 if a node $j$ have a link pointing to node $i$ and zero otherwise. The columns with only zero elements (*dangling nodes*) are replaced by columns with $1/N$ where $N$ is the matrix size. The elements of other columns are renormalized in such a way that their sum becomes equal to unity ($\sum_i S_{ij} = 1$, $S_{ij} = A_{ij}/\sum_i A_{ij}$). Thus we obtain the matrix $S_{ij}$ of Markov transitions. Then the Google matrix $G$ of the network takes the form [6, 7]:

$$G_{ij} = \alpha S_{ij} + (1-\alpha)/N. \quad (1)$$

Here, the damping factor $\alpha$ is taken in the range $0 < \alpha \leq 1$. In the context of the World Wide Web (WWW) the term $(1-\alpha)$ describes for a random surfer a probability to jump on any node of the network. The above construction of $G$ has been proposed by Brin and Page [6] to describe the structure of the World Wide Web (WWW). For the WWW it is assumed that the Google search engine uses $\alpha \approx 0.85$ [7]. We can also consider a generalized case of weighted Markov transitions $S_{ij}$ corresponding to real positive elements of $A_{ij}$ like happens for the world trade network (see e.g. [8]).

The matrix $G$ belongs to the class of Perron-Frobenius operators, its largest eigenvalue is $\lambda = 1$ and other eigenvalues have $|\lambda| \leq \alpha$ [7, 9]. The right eigenvector at $\lambda = 1$, which is called the PageRank ($GP = P$), has real nonnegative elements $P(i)$ and gives a probability $P(i)$ to find a random surfer at site $i$. It is possible to rank all nodes in a decreasing order of PageRank probability $P(K(i))$ so that the PageRank index $K(i)$ counts all $N$ nodes $i$ according their ranking, placing the most popular nodes at the top values $K = 1, 2, 3....$ Usually for many real directed networks the distributions of number of ingoing and outgoing links are described by a power law (see e.g. [10]), generating an average approximately algebraic decay of PageRank probability $P(K) \propto 1/K^{\beta}$ with $\beta \approx 0.9$. Some examples of directed networks can be found in [11].

It is important to note that matrices of Google class practically have not been studied in physical systems even if they naturally appear in the frame of Ulam networks generated by the Ulam method for dynamical maps in a coarse-grained phase space (see e.g. [12–14]).

Therefore, it is interesting to see if the phenomena of Anderson localization and Anderson delocalization transition can appear for Google matrices. Certain indications on a possible Anderson transition for the Ulam networks, built from dissipative maps, have been reported

* Corresponding author E-mail: dima@irsamc.ups-tlse.fr
[1] Budker Institute of Nuclear Physics, 630090 Novosibirsk, Russia
[2] Novosibirsk State University, 630090 Novosibirsk, Russia
[3] Laboratoire de Physique Théorique du CNRS (IRSAMC), Université de Toulouse, UPS, F-31062 Toulouse, France

in [12] with more detailed discussions presented in [11]. Thus, it would be useful to find random matrix models which are able to reproduce typical properties of spectrum and PageRank decay in real directed networks. However, the results presented in [15] show that the full matrix $G$ with random matrix elements have an unrealistic spectrum and hence other random matrix models of $G$ should be developed. The models discussed in [16] give certain indications of delocalization of eigenstates of $G$ but the spectrum of $G$ in these models has a large gap and is very far from the spectra of real directed networks. With this aim we describe below a number of random Google matrix models and analyze the properties of their spectra and eigenstates. We use certain spectral properties of small size *orthostochastic* matrices with $N = 3, 4$ established in [17].

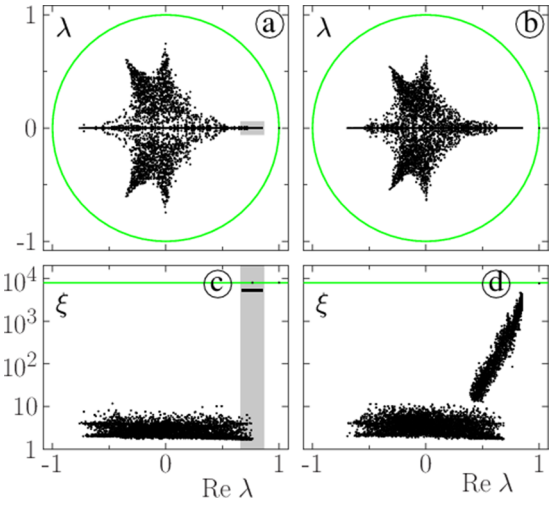


**Figure 1** Google matrix eigenvalues λ (a,b), and IPR $\xi$ of eigenvectors as a function of Reλ (c,d). Panels show data for RMZ3 model (Sec. 2.1) at fixed amplitudes $\varepsilon_i = 0.5$ (a,c) and for random amplitudes $0.15 \leq \varepsilon_i \leq 0.3$ (b,d). The green circle shows $|\lambda| = 1$ (a,b); the green horizontal line shows maximal possible $\xi = N$ (c,d); the gray band in (a,c) highlights specific states (see text). Here the total number of nodes is $N$=8000.

## 2 Random matrix models of G

We start from a description of various random matrix models of Google matrix $G$ presenting the results of their spectral properties in next Section.

### 2.1 Model RMZ3: random three-diagonal blocks

Following [17] we consider *orthostochastic* matrix blocks $B_{ij}$ of size $M \times M = 4 \times 4$. The *orthostochastic* property means that $B_{ij} = {O_{ij}}^2$, where an orthogonal matrix $O$ has random matrix elements obtained via random rotations. Since $O$ is an orthogonal matrix the matrix $B$ is bistochastic with $\sum_i B_{ij} = \sum_j B_{ij} = 1$ [17]. The main reason to use such blocks $B$ is a similarity of complex spectrum of random matrix ensemble of $B$ with the spectrum of $G$ of university networks of Cambridge and Oxford, as discussed in [11]. The size $4 \times 4$ can be considered as preferential random links between a group of 4 friends. However, a weak point of the random ensemble of $B$ [17] is a small matrix size $N = 4$, while for the above universities we have $N \approx 2 \times 10^5$.

To go to large values of $N$ in matrix $S_{ij}$ we construct the **Random Matrix model** $Z3$ **(RMZ3)** as follows: we place blocks $B$ of size $M = 4$ on the main diagonal with weights $(1 - \varepsilon_i)$ and on two adjacent upper and lower diagonals with weight $\varepsilon_i/2$, where $\varepsilon_i$ $(i = 1, \ldots, N/M)$ are random numbers uniformly distributed in some interval $(\varepsilon_{min}, \varepsilon_{max})$; each block represents a random realization of $B$; then the matrix $G$ of total size $N$ is built from $S$ via the equation (1). Here we consider two cases with a constant $\varepsilon_i = 0.5$ and the interval range $0.15 \leq \varepsilon_i \leq 0.3$ (see Fig. 1). Obviously, by construction the final matrix belongs to the Google matrix class. We use notations $S_Z$ and $G_Z$ for the matrices $S$ and $G$ of this model.

### 2.2 Model RMZ3S: RMZ3 with shortcuts

The model **RMZ3S** is obtained from RMZ3 by adding shortcut links between blocks $B$ in the upper triangle of the whole matrix $S$, the blocks of shortcut links are placed randomly in this part of $S$. The amplitude of transitions from one block to another block (outside of three-diagonal blocks of RMZ3) is taken at some fixed value $\varepsilon_s$. The shortcut blocks are randomly and uniformly distributed over the upper triangle of the whole matrix. *After* adding the shortcut blocks the columns affected by shortcut blocks are renormalized to unity. In this way the obtained matrix $S$ again belongs to the Google matrix class. The blocks of shortcuts are placed randomly in the upper triangle of matrix $S$, their number $N_s$ is determined by the parameter $\delta = 4N_s/(3N)$. In fact $\delta$ gives the ratio of shortcut blocks to the number of blocks $3N/4$ in the model RMZ3. Again each block $B$ in the main three-diagonal part of RMZ3 and blocks at shortcut positions are taken as random and independent realizations for each block. We note that the shortcuts between single nodes have been used for studies of quantum chaos and Anderson transition in the small world Anderson model

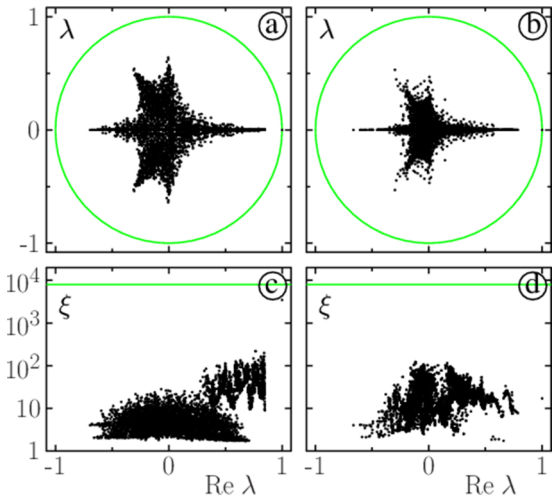


**Figure 2** Same as in Fig. 1 for RMZ3S model (Sec. 2.2) with $0.15 \leq \varepsilon_i \leq 0.3$, shortcut amplitude $\varepsilon_s = 0.3$, $\delta = 0.1$ (a,c) and $\delta = 1$ (b,d). Here $N = 8000$.

(see [11, 18, 19]). The results for RMZ3S model are shown in Figs. 2, 3.

### 2.3 Model RMZ3F: RMZ3 plus triangular matrix

The results obtained in [15, 20] show that a triangular matrix of Google matrix class has a tendency to have a realistic PageRank probability decay with $P \propto 1/K$ and have some eigenvalues of finite amplitudes $|\lambda|$. Due to these indications we construct a matrix $S_F$ in the following way: $N_u$ random numbers $f_i$ from the interval $(0, 1)$ are placed on random positions of the upper triangle of matrix of size $N$, then all columns are renormalized to unity and columns with all zero elements are replaced by columns with all elements $1/N$. Then we construct the matrix $G$ of the **model RMZF** as:

$$S_{ZF} = (1-\mu)S_Z + \mu S_F\,,\quad G_{ZF} = \alpha S_{ZF} + (1-\alpha)/N\,. \qquad (2)$$

Here $\mu$ determines a measure of contribution of $S_F$ with $0 < \mu < 1$. The number of nonzero random elements $N_u$ is given by parameter $\delta = N_u/(12N)$. The results for the RMZF model are shown in Figs. 3, 4, 5.

### 2.4 Anderson models AD2 and AD3 for G matrix

We use the usual Anderson model [1, 3] with diagonal disorder terms $W_i$ and transitions $V$ to nearby sites on a

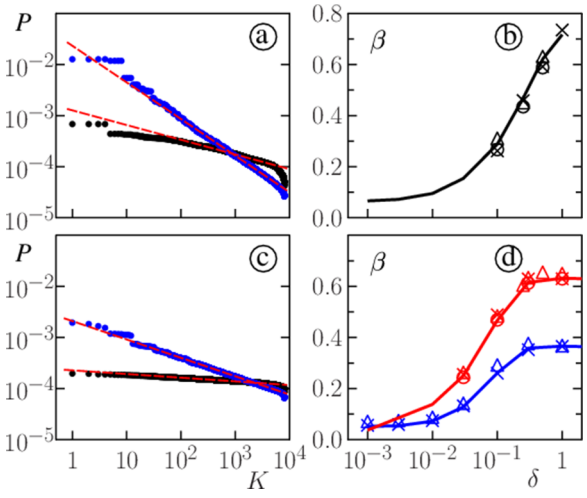


**Figure 3** Dependence of $P(K)$ for models RMZ3S (Sec. 2.2) in panels (a,b) and RMZ3F (Sec. 2.3) in panels (c,d); here $0.15 \leq \varepsilon_i \leq 0.3$. In panel (a) we have $\delta = 0.1$ (black symbols) and $\delta = 1$ (blue symbols) at $N = 8000$; the fitted algebraic dependence is shown by straight dashed lines with parameters: $a = -6.67$, $\beta = 0.288$ at $\delta = 0.1$ and $a = -3.76$, $\beta = 0.71$ at $\delta = 1$; panel (b) shows the dependence of $\beta$ on $\delta$ with the full curve for $N = 8000$ and triangles, crosses and circles for $N = 2000, 4000, 16000$ respectively; the amplitude of shortcut elements is $\varepsilon_s = 0.3$. In panel (c) we have $\delta = 0.01$ (black symbols) and $\delta = 3$ (blue symbols) at $\mu = 0.1$ and $N = 8000$; the fitted algebraic dependence is shown by straight dashed lines with parameters: $a = -8.39$, $\beta = 0.072$ at $\delta = 0.01$ and $a = -6.17$, $\beta = 0.36$ at $\delta = 3$; panel (d) shows the dependence of $\beta$ on $\delta$ for $\mu = 0.1$ (blue) and $\mu = 0.3$ (red) with the full curves for $N = 8000$ and triangles, crosses and circles for $N = 2000, 4000, 16000$ respectively.

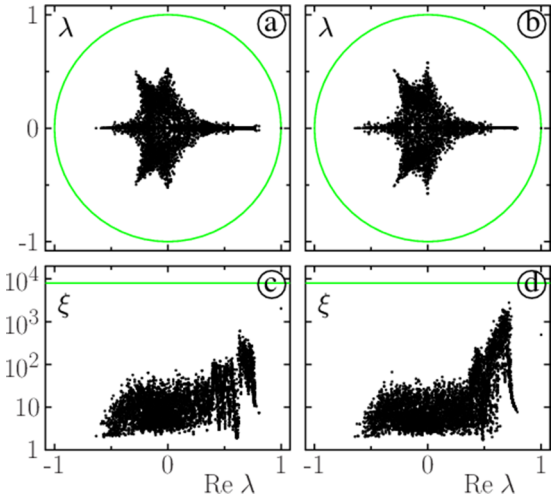


**Figure 4** Spectrum (a,b) and IPR $\xi$ dependence of Re$\lambda$ for the model RMZ3F (Sec. 2.3) at $\delta = 0.1$ (a,c) and $\delta = 3$ (b,d); here $0.15 \leq \varepsilon_i \leq 0.3$, $\mu = 0.1$, $N = 8000$; circle and horizontal lines are as in Fig. 1.

Original Paper

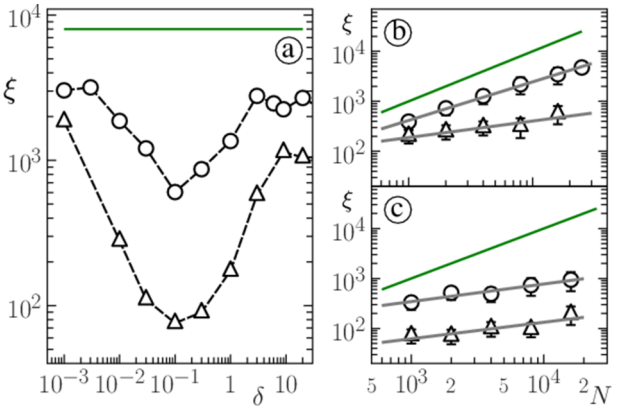


**Figure 5** Panel (a) shows dependence of maximal IPR $\xi$ (for states with $|\lambda| < 1$) on parameter $\delta$ for the model RMZ3F (Sec. 2.3) at $N = 8000$. Dependence of maximal IPR $\xi$ on $N$ is shown in panels (b) at $\delta = 3$ and (c) at $\delta = 0.1$; error bars show statistical error, if it is larger than symbol size, obtained from $N_r$ disorder realizations. We use $N_r = 11$ at $N = 2000$, $N_r = 8$ at $N = 4000$, $N_r = 4$ at $N = 8000$, $N_r = 3$ at $N = 16000$. In all panels $\mu = 0.1$ (circles) and $\mu = 0.3$ (triangles), $0.15 \leq \varepsilon_i \leq 0.3$; the straight green lines show dependence $\xi = N$; the straight gray lines in (b,c) show the fitted dependence (see text).

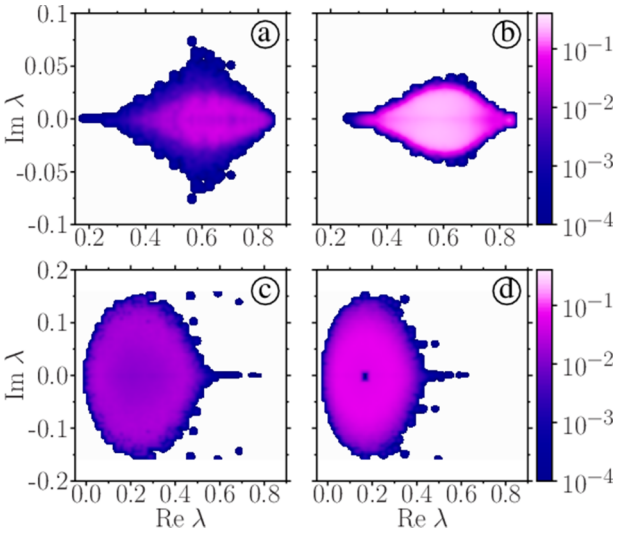


**Figure 6** Distribution of IPR $\xi_i$ on $\lambda-$plane for the Anderson type models AD2 at $d = 2$ (a) and AD3 at $d = 3$ (b) (Sec. 2.4) and the Anderson type models with shortcuts AD2S (c) and AD3S (d) at $\delta = 2$ (Sec. 2.5). Here $\varepsilon_{max} = 0.6$; $N = 130^2 = 16900$ for (a,c); $N = 25^3 = 15625$ for (b,d) and $\varepsilon_{max} = 0.6$, $\varepsilon_s = \varepsilon_{max}/2 = 0.3$ for (c,d). Color bars show the ratio $\xi_i/N$ (IPR values are averaged inside cells of coarse-grained lattice $60 \times 60$).

lattice in dimension $d$:

$$W_{\mathbf{i}}\psi_{\mathbf{i}} + V\psi_{\mathbf{i+1}} + V\psi_{\mathbf{i-1}} = \lambda\psi_{\mathbf{i}} \,, \qquad (3)$$

where indexes in bold are vectors in $d$-dimensional space. On the basis of (3) we construct the matrices $S$ and $G$.

Thus we consider the dimensions $d = 2, 3$ corresponding to square and cubic lattices. The matrix $S$ is constructed as follows: each transition matrix element, corresponding to $V$ terms, in the Anderson model in dimension $d$ (3) is replaced by a random number $\varepsilon_i$ uniformly distributed in the interval $[0, \varepsilon_{max}/2d]$, the diagonal element $W_i$ is replaced by unity minus the sum of all $\varepsilon_i$ over $2d$ nearby sites $(1 - \sum_{i=1}^{2d} \varepsilon_i)$. The asymmetric matrix $S$ constructed in this way belongs to the Google matrix class. Thus we obtain the matrices $S_{AD2}$, $G_{AD2}$ for the **model AD2** and $S_{AD3}$, $G_{AD3}$ for the **model AD3** for $d = 2$ and 3 respectively. The results for these models are presented in Figs. 6, 7, 9.

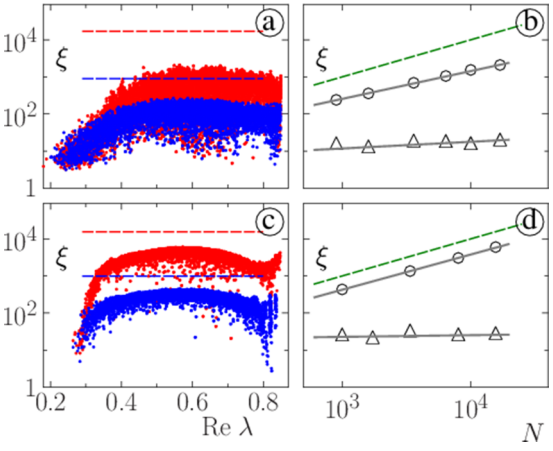


**Figure 7** Dependence of $\xi$ on $\mathrm{Re}\lambda$ (a,c) and $\xi$ on $N$ (b,d) for the models AD2 (a,b) and AD3 (b,d) (see Sec. 2.4). For AD2: panel (a) is for $N = 900$ (blue, $N_r = 10$ realizations) and $N = 16900$ (red, $N_r = 1$); panel (b) shows dependence $\xi(N)$ with fits $\xi \propto N^{\nu}$ for eigenstates at the spectrum edge with $\mathrm{Re}\lambda = 0.23 - 0.25$ (triangles, $\nu = 0.18$) and for maximal $\xi$ (circles, $\nu = 0.75$). For AD3: panel (c) is for $N = 1000$ (blue, $N_r = 10$ realizations) and $N = 15625$ (red, $N_r = 1$); panel (d) shows dependence $\xi(N)$ for eigenstates at the spectrum edge with $\mathrm{Re}\lambda = 0.23 - 0.25$ (triangles, $\nu = 0.05$) for maximal $\xi$ (circles, $\nu = 0.95$). Here $\varepsilon_{max} = 0.6$. The fits are shown by gray lines, green (b,d) and blue, red (c,d) dashed lines show dependence $\xi = N$. For panels (b,d) the number of realizations changes from $N_r = 10$ to 3 when $N$ changes from minimal to maximal value.

## 2.5 Anderson models AD2S and AD3S with shortcuts

By adding shortcut links between pairs of nodes randomly distributed in the upper triangle of matrix $S$ we obtain **models AD2S and AD3S** respectively from models AD2 and AD3. The number of shortcut elements in

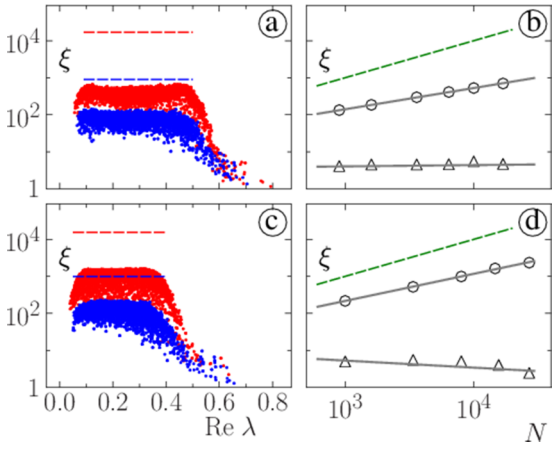


**Figure 8** Same as in Fig. 7 but for the models AD2S (a,b) and AD3S (c,d) (see Sec. 2.5) at $\delta = 2$; all parameters are as in Fig. 7. The fits give: (b) $\nu = 0.04$ at the spectrum edge around $\mathrm{Re}\lambda \approx 0.6$ (triangles), $\nu = 0.57$ for maximal $\xi$ (circles); (d) $\nu = -0.19$ at the spectrum edge around $\mathrm{Re}\lambda \approx 0.6$ (triangles), $\nu = 0.73$ for maximal $\xi$ (circles). Here $\varepsilon_{max} = 0.6$, $\varepsilon_s = \varepsilon_{max}/2 = 0.3$. For panel (b) [(d)] the number of realizations changes from $N_r = 10$ to 3 [1] when $N$ changes from 900 to 16900 [27000].

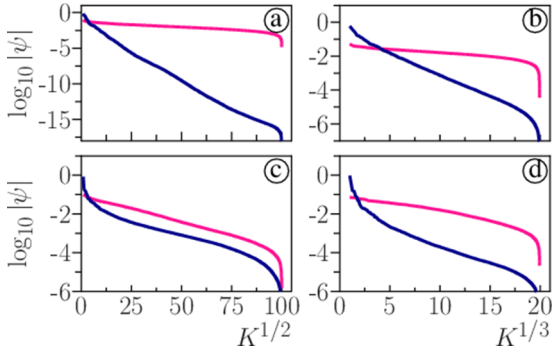


**Figure 9** Dependence of eigenvector amplitudes $|\psi|$ on their rank index $K$ for models AD2 (a), AD3 (b) from (Sec. 2.4) and AD2S (c), AD3S (d) from (Sec. 2.5). Here $\delta = 0$ for (a,b) and $\delta = 2$ for (c,d); $N = 10^4$ for (a,c) and $N = 20^3$ for (b,d). We use $\varepsilon_{max} = 0.6$ and $\varepsilon_s = 0.3$ in (c,d). Data show maximally delocalized (maximal $\xi$ corresponding to PageRank, magenta upper curve) and maximally localized (smallest $\xi$, blue bottom curve) eigenstates.

$S$ is taken to be $N_s = 2dN\delta$, their amplitude is taken as $0 \le \varepsilon_i \le \varepsilon_s = \varepsilon_{max}/2$, after adding shortcuts the columns with shortcut elements are renormalized to unity. Thus the sum of elements in each column is equal to unity and $S$ belongs to the Google matrix class. We note the matrices of these models as $S_{AD2S}$, $G_{AD2S}$, $S_{AD3S}$, $G_{AD3S}$ respectively for $d = 2, 3$. The results for these models are presented in Figs. 8, 9, 10.

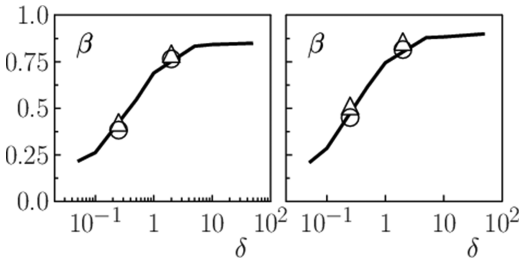


**Figure 10** Dependence of the PageRank exponent $\beta$ on the parameter $\delta$ for the models AD2S (left panel) and AD3S (right panel). Left panel: the solid curve shows data for $N = 80^2$, with triangles for $N = 40^2$ and circles for $N = 130^2$. Right panel: the solid curve shows data for $N = 20^3$, with triangles for $N = 10^3$ and circles for $N = 25^3$. Here $\varepsilon_{max} = 0.6$ and $\varepsilon_s = 0.3$.

## 2.6 Anderson models AD2Z and AD2ZS with blocks and block shortcuts

By replacing matrix elements in the model AD2 by blocks $B$ of size $4 \times 4$ (see Sec. 2.1) we obtain the **model AD2Z**. In a similar way for the model AD2S we obtain the **model AD2ZS** with block shortcuts. In this case we restrict our studies only for dimension $d = 2$ since the matrix size becomes too large for $d = 3$. Amplitudes $\varepsilon_{max}$ and $\varepsilon_s$ are defined as for the models AD2 and AD2S. Since the transitions are now given by blocks then the parameter $\delta$ is now defined as $N_s = 2d(N/4)\delta$ with $d = 2$. The results for models AD2Z and AD2ZS are presented in Figs. 11, 12.

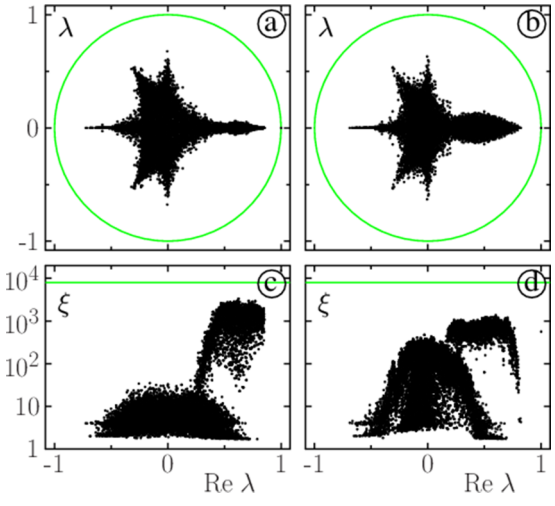


**Figure 11** Spectrum $\lambda$ (a,b) and IPR $\xi$ vs. $\mathrm{Re}\lambda$ (c,d) for the models AD2Z (a,c) and AD2ZS at $\delta = 0.25$ (b.d) from Sec. 2.6. Here $N = 4 \times 70^2 = 19600$, $\varepsilon_{max} = 0.6$ and $\varepsilon_s = 0.3$ in (c,d).

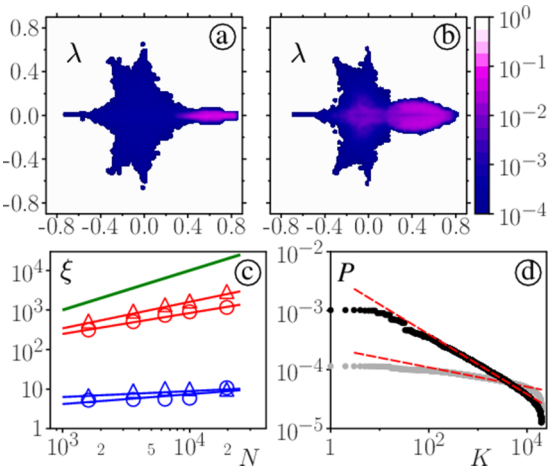


**Figure 12** Top panels show distribution of IPR $\xi$ values on $\lambda-$plane for models AD2Z (a) and AD2ZS at $\delta = 0.25$ (b) of Sec. 2.6 with parameters of Fig. 11; color bar gives the ratio $\xi/N$ obtained from cells as in Fig. 6. Panel (c): dependence of $\xi$ on $N$ for AD2Z with triangles for states with $\lambda$ located in the delocalized domain $\mathrm{Re}\lambda \in (0.3, 0.85)$ (red triangles, fit gives $\nu = 0.67$) and in the localized domain $\mathrm{Re}\lambda < -0.5$ (blue triangles, $\nu = 0.15$); for AD2ZS at $\delta = 0.25$ with circles for states with $\lambda$ located in the delocalized domain $\mathrm{Re}\lambda \in (0.2, 0.85)$ (red circles, $\nu = 0.53$) and in the quasi-localized domain $\mathrm{Re}\lambda < -0.5$ (blue circles, $\nu = 0.25$); fits are shown by lines, green line shows $\xi = N$. Panel (d): dependence of PageRank probability $P$ on PageRank index $K$ for models AD2Z (gray symbols) and AD2ZS at $\delta = 0.25$ (black symbols); the fits for the range $K \in (100, 6000)$ are shown by dashed lines with $\beta = 0.16$ (AD2Z) and $\beta = 0.51$ (AD2ZS) for the parameters of panels (a,b).

## 3 Spectral properties of G matrix models

We use exact numerical diagonalization for analysis of spectrum and eigenstates of models of Sec. 2. The matrix size $N$ is changed from a minimal $N = 900$ up to maximal $N = 27000$. For the description of the decay of PageRank probability we use a fit $\ln P = a - \beta \ln K$ which gives us the PageRank exponent of algebraic $\beta$. In all simulations we use $\alpha = 0.85$. The right eigenstates $\psi_i(j)$ of $G$ are determined by

$$\sum_{j'=1}^{N} G_{jj'}\psi_i(j') = \lambda_i\psi_i(j) \ . \qquad (4)$$

We characterize $\psi_i(j)$ by the Inverse Participation Ratio (IPR) $\xi_i = (\sum_j |\psi_i(j)|^2)^2/\sum_j |\psi_i(j)|^4$. This quantity is broadly used in the studies of Anderson localization [3] and determines the number of sites effectively populated by an eigenstate. The value of $\xi$ is independent of normalization. We use normalization $\sum_i P(i) = 1$ for the PageRank eigenstate at $\lambda = 1$. For each eigenvector $\psi_i(j)$ we can order all nodes in a monotonically decreasing order of $|\psi_i(j)|$ thus obtaining the local rank index $K$ for a given $\psi_i(j)$. Such a ranking was used in [21, 22].

We note that in the following Figs. when we show the dependence of $\xi$ on $Re\lambda$ then all $\lambda$ values are shown; we use various number of disorder realizations which is given in figure captions or equal to one if not directly stated (but we checked that the results are not sensitive to a change of disorder realization).

In the following we present analysis of right eigenstates of $G$ which produce influence on the PageRank vector. The properties of left eigenvectors reserve a separate analysis (e.g. the left eigenvector at $\lambda = 1$ has constant equal elements since the sum of each column elements is equal to unity).

Below we describe the results for models of Sec. 2.

### 3.1 Results for RMZ3 model

For the model RMZ3 at $\varepsilon_i = const = 0.5$ the spectrum is shown in Fig. 1a. We see that it has a form of 6−rays star typical for the directed networks studied in [11, 21, 22]. The size of the star is slightly reduced since all $\lambda_i(\alpha) \to \alpha\lambda_i(\alpha = 1)$ for $\alpha < 1$, except $\lambda = 1$ [7]. There is also additional reduction of $|\lambda_i|$ due to finite coupling terms $\varepsilon_i > 0$ but this reduction is moderate and the spectrum of $G_Z$ is close to the spectrum of independent $4 \times 4$ blocks found in [17]. Thus RMZ3 model captures a part of real properties of directed networks.

An interesting property of eigenstates becomes visible from the dependence of $\xi$ on $\mathrm{Re}\lambda$ shown in Fig. 1c at $\varepsilon_i = 0.5$. Many eigenstates have relatively small $\xi < 10$ which remain bounded with the increase of $N$ up to $N = 16000$ (data not shown). However, there is a group of states (gray band) with $\xi \sim N$ growing linearly with $N$ (data not shown). These are delocalized states. Their origin becomes clear from the following consideration. We can use the anzats in which the elements of $\psi(j)$ are constant inside a given block $B_m$ with a values $\varphi_m$. Then Eq.(4) takes the form

$$(1-\varepsilon)\varphi_m + \varepsilon(\varphi_{m+1} + \varphi_{m-1})/2 = \lambda\varphi_m \ , \qquad (5)$$

since the matrix $G$ is bistochastic with sum of elements in rows being unity since $\varepsilon_i = const$. The spectrum $\lambda$ in (5) is real. Thus we obtain in (5) the Bloch equation with plane wave delocalized solutions well known for crystals [2, 3]. These solutions belong to the gray band part of the spectrum in Fig. 1a. Another part of the spectrum

corresponds to such $\psi(j)$ which have different values on a scale of one block $B$.

The case with different $\varepsilon_m$ (e.g. $0.15 \leq \varepsilon_m \leq 0.3$ in Fig. 1b,d) we can use the same anzats for the left vector $\varphi_m$ that leads to the eigenvalue equation:

$$(1-\varepsilon_m)\varphi_m + \varepsilon_m(\varphi_{m+1}+\varphi_{m-1})/2 = \lambda\varphi_m. \quad (6)$$

Such a problem corresponds to the case of off-diagonal disorder in the $1d$ Anderson model where the localization length, and hence IPR, is diverging at the center of the band [2, 3]. The spectrum $\lambda$ in (6) is real. A similar problem is known as the Sinai walk [23] where transition probabilities on a Markov chain are fluctuating. This model has been studied extensively (see e.g. [24] and Refs. therein).

The spectrum $\lambda$ in (6), corresponding to this anzats, is the same for the right eigenvectors [7]. The right eigenvectors are different from the left ones but have a similar structure on average. The IPR values, shown in Fig. 1d are significantly reduced, comparing to the case $\varepsilon_m = const$, except those with $\lambda$ close to unity. When $N$ is increasing we find that IPR is growing only for $\lambda \to 1$ while for $|\lambda| < 1$ IPR values remains finite. This corresponds to the known results for the Anderson model with off-diagonal disorder. Other eigenstates for which $\psi_i$ is not constant inside $B$ blocks correspond to the eigenstates with rather small IPR values $\xi \sim 10$.

Even if the spectrum and eigenstates have interesting properties in the two above cases of model RMZ3 there is a weak point here: the PageRank probability $P$ in these cases is flat being practically independent of $K$ and $\xi \sim N$. Thus the situation is very different from the real directed networks with $\beta \approx 1$ (see e.g. [7, 11]). This happens due to a space homogeneous structure of the matrix $G$ (a part of fluctuations) and thus there is no leading node with a large number of links. Due to that we try to introduce shortcut links as described in the next Sec. 3.2.

### 3.2 Properties of RMZ3S model

The spectrum and IPR dependence for RMZ3S model with shortcuts are shown in Fig. 2 for two typical values of parameter $\delta$. We see that at small values of $\delta$ (e.g. $\delta = 0.1$) the spectrum structure is practically the same as for RMZ3 model. However, for larger values ( $\delta = 1$) the size of the spectrum star is decreasing. The values of IPR are significantly reduced at finite values of $\delta$ and our data show that the maximal $\xi$ values remain less than $\xi = 200$ even for the largest size $N = 16000$ for $0.1 \leq \delta \leq 1$ for all $|\lambda| < 1$ (data not shown). Thus in this model all eigenstates remain localized.

Even if all states are localized the decay of PageRank is more close to the case of real directed networks. Indeed, the data of Fig. 3a,b show that $P(K)$ have approximately algebraic decay with PageRank index. The fit allows to determine the PageRank exponent $\beta$ which is small at $\delta \sim 0.1$ and is growing with increase of $\delta$ reaching values $\beta \approx 0.75$ at $\delta = 1$. It is important to note that $\beta$ is independent of $N$ at large $N$ values. Thus the homogeneous random elements in the upper triangle of $S$ matrix allow to obtain $\beta$ close to unity at large $\delta$. Indeed, in the limit of rather large $\delta$ we come to the case of triangular matrix $S$ studied in [15] (and also in [20]) where one obtains an approximate decay $P \propto 1/K$. Indeed, at large $\delta$ a sum of elements in a row of $G$ drops approximately as $1/K$ (where $K$ is a row index) leading to $P \propto 1/K$. Indeed, we can say that $P(K) \approx \sum_j G_{Kj} e_j \sim 1/K$, where $e_j = 1/N$ is a homogeneous initial vector, considering this as one iteration of the PageRank algorithm [7]. We note that for the PageRank vector we have $\xi \sim N$ for $\beta < \beta_c = 1/4$.

Thus the model RMZ3S has a reasonable spectrum structure and an algebraic PageRank probability decay. But all eigenstates with $|\lambda| < 1$ remain localized. Thus we go to the analysis of RMZ3F model.

### 3.3 Results for RMZ3F model

The spectrum and IPR values for the RMZ3F model are presented in Fig. 4. We see that the star spectrum structure is preserved but IPR values are increased in a vicinity $\mathrm{Re}\lambda \approx \alpha$. The examples of $P(K)$ and $\beta(\delta)$ dependencies are shown in Fig. 3c,d. It is important to note that $\beta$ is independent of $N$ at large $N$ values. Qualitatively, the situation is similar to the model RMZ3S but the effect of $\delta$ on localization properties of $\xi$ is more complicated.

Indeed, it is well seen in Fig. 5a that the maximal IPR values (excluding PageRank vectors) are at first reduced with an increase of $\delta$ from $10^{-3}$ up to 0.1 but they are increased when $\delta$ goes from 0.1 to 10. The dependence of maximal $\xi$ on $N$ at $\delta = 0.1; 3$ is shown in Fig. 5b,c for $\mu = 0.1; 0.3$. We fit this dependence by a power law $\xi \propto N^{\nu}$ and obtain for $\mu = 0.1$: $\nu = 0.352$ (at $\delta = 0.1$) and $\nu = 0.770$ (at $\delta = 3$); for $\mu = 0.3$: $\nu = 0.33$ (at $\delta = 0.1$ and 3). These results show that there are certain states (except PageRank) that become delocalized in the limit of large matrix size. In a certain sense, for the dependence $\xi(N)$ we have a certain similarity with the results obtained in [16] where a sub-polynomial growth of $\xi$ with $N$ has been found for randomized university networks and preferential attachment models. However, for the RZ3F model the

spectrum has no large gap and is more similar to the real directed networks.

The investigations of RMZ3F model at larger sizes (e.g. with the help of the Arnoldi method [11, 21]) can provide a more firm conclusion about the delocalization properties of eigenstates in this model.

### 3.4 Properties of AD2 and AD3 models

The spectra of AD2 and AD3 models are shown in Fig. 6a,b with color plot of IPR values. We see that there are rather large values of $\xi$ indicating existence of delocalized eigenstates. Indeed, a more detailed analysis presented in Fig. 7 shows that for the states of the spectral range $\mathrm{Re}\lambda > 0.25$ IPRs are growing with $N$ clearly demonstrating delocalization. Indeed, for maximal $\xi$ from this range (excluding PageRank) we find $\nu = 0.75$ at $d = 2$ and $\nu = 0.95$ at $d = 3$. At the same time in a vicinity of the spectrum edge $\mathrm{Re}\lambda < 0.25$ we have $\nu = 0.18; 0.05$ for $d = 2; 3$ clearly showing that in this part of the spectrum the eigenstates are well localized. Indeed, for these localized states we have an exponential decay $\ln|\psi| \propto -K^{1/d}$ with the eigenstate rank index $K$ (see Fig. 9a,b). Such a decay also appears for the localized states of the Anderson model in dimension $d$.

But for the majority of eigenstates we have significant growth of $\xi$ with $N$ showing that these states are delocalized. Of course, the case of $d = 2$ should be studied in more detail since for the standard Anderson model at $d = 2$ (3) all eigenstates are exponentially localized [3]. However, we have here non-Hermitian matrix and for our knowledge there are no rigorous results about localization in such matrices in $d = 2$.

Even if in AD2, AD3 models we find delocalization, the PageRank in these models is practically flat due to absence of central node (see Fig. 9a,b). Another weak point of AD2, AD3 models is a relatively narrow distribution of eigenvalues with $|\mathrm{Im}\lambda| < 0.1$ and due to that we continue our analysis with the next model.

### 3.5 Results for AD2S and AD3S models

The spectra of AD2S, AD3S models are shown in Fig. 6c,d. We see that the additional terms in upper triangle of matrix $S$ produce a broadening of $\mathrm{Im}\lambda$ which however still remains relatively narrow ($|\mathrm{Im}\lambda| < 0.2$). The IPR values are growing with $N$ except of the eigenstates at the spectral edge $\mathrm{Re}\lambda \approx 0.6$ (see Fig. 8). For these localized states the exponent $\nu$ is practically zero while for the maximal IPR (except PageRank) we find rather large values of $\nu = 0.57$ at $d = 2$, $\nu = 0.73$ at $d = 3$. Thus, in these models we clearly have the Anderson type transition from localized to delocalized eigenstates.

In analogy with the 3d Anderson model [3], we make a conjecture that in models AD2, AD3, AD2S, AD3S there is a certain mobility edge curve in the complex plane $\lambda$ which separates localized from delocalized states. In a qualitative manner such a curve is visible in Fig. 6 as a border between blue color of localized states with small $\xi$ and white color of states with large $\xi$. But definitely more detailed studies are required for a more exact determination of such a mobility edge curve.

Examples of PageRank probability decay are shown in Fig. 9. The new element, appearing in AD2S, AD3S models (comparing to AD2, AD3 cases), is a dependence of the PageRank exponent $\beta$ on the parameter $\delta$ as shown in Fig. 10. These data demonstrate that $\beta$ increases from $\beta \approx 0.2$ at $\delta = 0.1$ up to $\beta \approx 0.9$ at $\delta = 3$. Thus AD2S,AD3S models have delocalized eigenstates and the PageRank exponent of real directed networks. The only weak point is a narrow distribution of spectrum in $\mathrm{Im}\lambda$. To improve this feature we study in next Section the models AD2Z, AD2ZS.

### 3.6 Results for AD2Z and AD3ZS models

The spectra of AS2Z, AD2ZS models are shown in Fig. 11. We see that the star structure appears due to introduction of blocks $4 \times 4$. The dependence of IPR $\xi$ on $\mathrm{Re}\lambda$ clearly shows the existence of two groups of states with small $\xi < 100$, presumably for localized phase, and large $\xi > 100$, presumably for delocalized phase.

The distribution of $\xi$ on $\lambda-$plane is shown in Fig. 12a,b. Again we see signs of the mobility edge curve separating localized (blue) and delocalized (white) eigenstates.

The dependence of $\xi$ on $N$ is shown in Fig. 12c. There are well localized states with $\xi$ practically independent of $N$ ($\xi < 20$) and delocalized states for which $\xi$ is growing with $N$ with a relatively large growth exponent $\nu = 0.67$ at $\delta = 0$ and $\nu = 0.53$ at $\delta = 0.25$. This gives a strong argument for existence of the Anderson transition with a mobility edge in a complex $\lambda-$plane in these models.

The decay of PageRank probability is shown in Fig. 12d: at $\delta = 0$ we have a flat $P(K)$ distribution with the exponent $\beta = 0.16$, while at $\delta = 0.25$ we find $\beta = 0.51$ being close to the values found in real directed networks (e.g. for the Twitter network $\beta \approx 0.54$ [11]).

Thus we can say that the model AD2ZS is the one being most close to real directed networks with the number of interesting features: algebraic decay of PageRank

probability with the exponent $\beta \approx 0.5$, absence of spectral gap at $\alpha = 1$, a broad star like distribution of eigenvalues in the complex $\lambda-$plane, existence of localized and delocalized eigenstates of the Google matrix with strong indications on the Anderson transition and the mobility curve in $\lambda-$plane.

Of course, the presented results are obtained for matrices of finite size while the Anderson delocalization assumes that states are delocalized over an infinite system size. Due to that the finite matrix simulations give only numerical indications. However, the clear increase of $\xi$ values with matrix size $N$, shown in Fig. 7, 8, 12, gives us a convincing evidence on existing delocalized states in the limit $N \to \infty$. The same Figs. demonstrate existence of localized states with $\xi$ being practically independent of $N$.

We expect that a similar model AD3ZS constructed in dimension $d = 3$ from the AD3S model will have even stronger delocalization properties.

## 4 Summary

Let us now summarize results obtained above in various models. We see that with the Anderson type models without shortcuts (AD2, AD3, AD2Z) we obtain delocalized eigenstates for a certain domain of eigenvalues $\lambda$ and localized eigenstates at the border of spectrum or at some regions of spectrum. The most interesting model is AD2Z with a broad domain of complex $\lambda$ (Fig. 12) while for the models AD2, AD3 the imaginary part of $\lambda$ is relatively small (Fig. 6). For the AD2Z model we have a clear separation between well localized states and those with large $\xi$ corresponding to delocalized domain. A certain curve (a contour) in the complex plain of $\lambda$ separates these two domains playing the role of mobility edge curve in the complex plain. However, a weak point of model AD2Z is a relatively small value of PageRank exponent $\beta \approx 0.16$. It is possible that more realistic values of $\beta \sim 0.5$ can be reached considering higher dimensions $d = 3, 4, ...$ with the transition blocks used in AD2Z. However, a verification of this expectation requires more advanced numerical simulations in future, probably with the help of the Arnoldi method described in [11].

Another promising case is the AD2ZS model with shortcuts. A small fraction of shortcuts added allows to increase the PageRank exponent and obtain $\beta \approx 0.5$ as in real networks. Even if shortcuts produce transitions to faraway nodes their effect has two tendencies. The first tendency is the delocalization effect since probability can be transferred to nodes located very far. But this does not necessary gives a delocalization since the wave function still can remain located on a small number of nodes with a relatively small $\xi$ values. Such a situation has been seen in the Anderson small world model where a small fraction (density) of shortcuts did not affect localized states remaining with small $\xi$ values and Poisson statistics [18, 19]. The second tendency of shortcuts is related to the fact that they introduce a disorder that may enhance localization features, as it clearly happens in Fig. 5a.

We think that it can be very promising to study the extentions of models AD2Z and AD2ZS to higher dimensions $d$ and larger matrix sizes.

## 5 Discussion

In this work we described various random matrix models of the Google matrix of directed networks. Our results show that for certain models (like AD2ZS) we have an algebraic decay of PageRank probability with the exponent $\beta \sim 0.5$, absence of spectral gap at $\alpha = 1$, existence of the Anderson transition and mobility edge in the complex $\lambda-$ plane. We think that the further analysis of the models described here will allow to establish more close links between the Anderson delocalization phenomenon in disordered solids and delocalization of eigenstates of the Google matrix of directed networks.

**Acknowledgments.** We thank L.Ermann and K.M.Frahm for useful discussions. This research is supported in part by the EC FET Open project "New tools and algorithms for directed network analysis" (NADINE *No* 288956). The research of OVZ was partially supported by the Ministry of Education and Science of Russian Federation.

**Key words.** Markov chains, Anderson localization, Google matrix, PageRank.

## References

[1] P. W. Anderson, Phys. Rev. **109**, 1492 (1958).
[2] E. Akkermans and G. Montambaux, Mesoscopic Physics of Electrons and Photons (Cambridge University Press, Cambridge UK, 2007).
[3] F. Evers and A. D. Mirlin, Rev. Mod. Phys. **80**, 1355 (2008).
[4] A. Goetschy and S. E. Skipetrov, arXiv:1303.2880[math-ph] (2013).
[5] S. E. Skipetrov and I. M. Sokolov, Phys. Rev. Lett. **112**, 023905 (2014).
[6] S. Brin and L. Page, Comp. Networks ISDN Sys. **30**, 107 (1998).
[7] A. M. Langville and C. D. Meyer, Google's PageRank and Beyond: The Science of Search Engine Rankings (Princeton University Press, Princeton USA, 2006).

[8] L. Ermann and D. L. Shepelyansky, Acta Phys. Polonica A **120**(6A), A158 (2011).
[9] M. Brin and G. Stuck, Introduction to dynamical systems (Cambridge University Press, Cambridge UK, 2002).
[10] S. Dorogovtsev, Lectures on complex networks (Oxford University Press, Oxford UK, 2010).
[11] L. Ermann, K. Frahm, and D. L. Shepelyansky, arXiv:1409.0428[physics.soc-ph] (2014).
[12] O. V. Zhirov and D. L. Shepelyansky, Phys. Rev. E **81**, 036213 (2010).
[13] L. Ermann and D. L. Shepelyansky, Eur. Phys. J. B **75**, 299 (2010).
[14] L. Ermann and D. L. Shepelyansky, Eur. Phys. J. B **76**, 57 (2010).
[15] K. M. Frahm, Y.-H. Eom, and D. L. Shepelyansky, Phys. Rev. E **89**, 052814 (2014).
[16] O. Giraud, B. Georgeot, and D. L. Shepelyansky, Phys. Rev. E **80**, 026107 (2009).
[17] K. Zyczkowski, M. Kus, W. Slomczynski, and H.- J. Sommers, J. Phys. A: Math. Gen **36**, 3425 (2003).
[18] A. D. Chepelianskii and D. L. Shepelyansky, http://www.quantware.ups-tlse.fr/talks-posters/chepelianskii2001.pdf (2001).
[19] O. Giraud, B. Georgeot, and D. L. Shepelyansky, Phys. Rev. E **72**, 036203 (2005).
[20] K. M. Frahm, A. D. Chepelianskii, and D. L. Shepelyansky, J. Phys. A: Math. Theor. **45**, 405101 (2012).
[21] K. M. Frahm, B. Georgeot, and D. L. Shepelyansky, J. Phys. A: Math. Theor. **44**, 465101 (2011).
[22] L. Ermann, K. M. Frahm, and D. L. Shepelyansky, Eur. Phys. J. B **86**, 193 (2013).
[23] Ya. G. Sinai, Theor. Prob. Appl. **27**(2), 247 (1982).
[24] P. Le Doussal, J. Stat. Mech: Theor. Exp. **2009**(7), P07032 (2009).